

# Single-Molecule STED Microscopy with Photostable Organic Fluorophores\*\*

Robert Kasper, Benjamin Harke, Carsten Forthmann, Philip Tinnefeld,\*  
Stefan W. Hell,\* and Markus Sauer\*

In recent years, fluorescence microscopy techniques have been invented that are no longer fundamentally limited by diffraction despite using visible light focused by conventional optical elements.<sup>[1–7]</sup> Contrary to earlier attempts to improve the spatial resolution, such as near-field optics and aperture filters, all far-field fluorescence “nanoscopy” methods known to date rely on a judicious exploitation of selected fluorophore properties. In particular, all are based on utilizing a molecular mechanism that renders the fluorophores incapable of responding with fluorescence emission to excitation light. This fluorescence inhibition mechanism is implemented in the image formation in such a way that fluorophores that are closer than the diffraction limit emit sequentially in time and hence can be discerned.<sup>[8,9]</sup>

In stimulated emission depletion (STED) microscopy, fluorescence is inhibited by subjecting the dye molecules to an additional beam of light, thus inducing stimulated emission from the fluorescent state  $S_1$  to the ground state  $S_0$ . The

fluorophore remains dark because, even if it becomes excited by the excitation beam, it is instantly pushed back to the  $S_0$  state. For this darkening by stimulated emission to prevail over fluorescence, the intensity  $I_m$  of the stimulated emission beam has to be substantially higher than the threshold intensity  $I_s$  at which the maximum population of the fluorescent state  $S_1$  is 50%. Due to the fact that the population probability of  $S_1$  decreases nearly exponentially with the intensity of the stimulating (STED) beam, for intensities  $I_m \gg I_s$  the excited state  $S_1$  is essentially forbidden and the fluorophore confined to the  $S_0$  state (i.e., switched off). With representative optical cross sections of  $10^{-16} \text{ cm}^2$  and a typical lifetime of the excited state of a few nanoseconds, the intensities  $I_s$  required for effective darkening by STED are in the 3–10 MW  $\text{cm}^{-2}$  range.

In a typical single-beam scanning STED microscope, the regularly focused excitation beam is superimposed by a doughnut-shaped STED beam for stimulated emission. The STED-beam intensity at the doughnut crest ensures that all fluorophores remain dark, except the few molecules located in the proximity of the intensity minimum of the doughnut center. With  $I_m$  giving the maximum intensity at the doughnut crest, the diameter of the area in which the fluorophore is allowed to be bright is given by  $d \approx \lambda/[2NA(1 + I_m/I_s)^{0.5}]$ . Applying an intensity  $I_m \gg I_s$  confines the region in which the dye molecules are allowed to be bright to arbitrarily small  $d$ . In principle,  $d$  can reach the size of a molecule.

Due to the reduced excitation volume in STED microscopy, fewer molecules are registered on average at a given point in time, which means that these molecules can be separated from those that are allowed to emit earlier or later. Note that in this case, the position of the bright fluorophore is predefined through the known position of the doughnut center. Scanning the superimposed beams across the object provides time-sequential registration of all fluorophores at known positions. Clearly, scanning the beams a step further enables the registration of those nearby fluorophores that were kept dark or inactivated by STED in the preceding scanning step.

For this concept to work, the fluorophores inactivated by the STED beam must instantly recover when falling into the region of diameter  $d$ , in which emission is requested. This instant onset of its fluorescence capability is guaranteed if the fluorophore remains in the  $S_0$  or  $S_1$  state during the action of the excitation and STED beams. In particular, the dye must not have passed to a bleached or other long-lasting dark state. On the other hand, during the scanning process an excited

[\*] Prof. P. Tinnefeld, C. Forthmann  
Angewandte Physik–Biophysik and Center for NanoScience  
Ludwig-Maximilians-University  
Amalienstr. 54, 80799 Munich (Germany)  
E-mail: Philip.tinnefeld@lmu.de

Prof. S. Hell, Dr. B. Harke<sup>+</sup>  
Max Planck Institute for Biophysical Chemistry  
Am Faßberg 11, 37077 Göttingen (Germany)  
E-mail: shell@gwdg.de

Prof. M. Sauer  
Biotechnology and Biophysics  
Julius-Maximilians-University Wuerzburg  
Am Hubland, 97074 Wuerzburg (Germany)  
E-mail: m.sauer@uni-wuerzburg.de

Dr. R. Kasper<sup>+</sup>  
Applied Laser Physics and Laser Spectroscopy  
Bielefeld University  
Universitätsstr. 25, 33615 Bielefeld (Germany)

[+] These authors contributed equally to this work.

[\*\*] This work was supported by the Biophotonics Program of the BMBF/VDI (grant 13N9234) and the Nanosystems Initiative Munich (NIM). We thank R. Medda for providing labeled cells for bleaching experiments on microtubule networks. STED = stimulated emission depletion.

fluorophore is likely to undergo undesired transitions to higher excited states  $S_n$  ( $n > 1$ ) or triplet states  $T_n$  that may lead to photobleaching.<sup>[10–12]</sup> These transitions can be effected by both the excitation and the STED beam. Since the intensity of the latter determines the resolution  $d$  of a STED microscope, high photostability of fluorophores, especially under large STED-beam intensities, is desired.

Depending on its structure, each fluorophore exhibits a certain probability for populating the triplet states  $T_n$  by intersystem crossing. As the lowest triplet state  $T_1$  typically exhibits lifetimes in the microsecond time range, the population of this state can be elevated. Because the states  $T_n$  ( $n > 1$ ) are prone to irreversible follow-up reactions, their population is considered to concomitantly augment photobleaching.<sup>[10–12]</sup> Therefore, pulsed STED microscopy with sub-MHz repetition rates has been applied, which provides sufficient time for the molecules between subsequent excitation cycles to relax from the triplet state to the ground state prior to any potential excitation into higher states, that is, so-called T-Rex STED.<sup>[13]</sup> Photobleaching is one of the main limitations in related far-field high-resolution approaches, such as so-called “saturated structured illumination” microscopy.<sup>[5]</sup> Far-field optical nanoscopy techniques are poised to revolutionize the investigation of biological structures and processes. However, since the fluorophore transitions are key elements to overcoming the diffraction limit, the success of these techniques critically depends on the photophysical and photochemical properties of the fluorophores.

At the same time, advances in understanding the photo-physics of fluorophores have enabled improvement of photostability with the aid of a reducing and oxidizing system (ROXS).<sup>[14,15]</sup> Here, triplet states are rapidly depopulated and radical anions or cations are formed by reduction or oxidation with appropriate redox agents. The resulting reactive radical is then depopulated by the complementary redox reaction to return to the singlet ground state. Interestingly, this approach has not only substantially improved the photostability of a range of fluorophores, but also enabled the generation and control of the lifetime of transient dark states, which can be exploited for fluorescence nanoscopy methods based on switching the fluorescence capability of individual molecules.<sup>[16–20]</sup>

Herein, we show that the ROXS concept also significantly improves STED imaging by reducing photobleaching and increasing brightness. We compare STED measurements of single molecules and stained microtubules using ROXS conditions and commonly applied Mowiol embedding, and demonstrate a several-fold increase in photostability using ATTO647N as fluorophore. These findings allow us to image single molecules at substantially higher STED-beam intensities  $I_m$ . As a result, resolution scaling of STED microscopy can be demonstrated with single molecules in two dimensions with a doughnut-shaped STED beam and a resolution of  $<30$  nm in the lateral direction. At this length scale, distance fluctuations of the 60-base-pair (bp) DNA linker used to attach the fluorophores to the surface become significant. Comparative experiments with a short tether without DNA uncover an apparent increase in resolution of nearly 10 nm. The difference in apparent resolution is explained by the movement of the

DNA tether, which we treat as a rigid rod with its end diffusing on a hemisphere with a radius of 20 nm. The photostability improvement is also essential to carry out three-dimensional (3D) STED microscopy as well as repetitive STED imaging to reveal changes of molecular position in space.<sup>[21]</sup>

For many fluorophores, photobleaching occurs from transient metastable dark states, such as triplet states, or states that are populated through the triplet system. Thus, efficient depopulation of the triplet state is the key for prolonged survival of fluorophores under irradiation. The ROXS is based on the ability to depopulate triplet states by redox reactions (see Figure 1a). To repopulate the singlet ground state of the fluorophore, the ROXS contains both a reductant, such as ascorbic acid or Trolox, and an oxidant, such as methyl viologen or Trolox-quinone.<sup>[14,15]</sup> Dependent on the redox properties of the triplet state of the fluorophore, an electron transfer occurs yielding either a radical anion or radical cation. Oxygen is usually removed enzymatically due to its high reactivity.

We first compare STED microscopy for samples embedded in the ROXS and in Mowiol. Mowiol was used for comparison since it has been extensively utilized in the STED microscopy of cellular structures.<sup>[22,23]</sup> ATTO647N was used as reference fluorophore due to its suitability for STED and for single-molecule fluorescence experiments.<sup>[10,14,21]</sup> Figure 1b–g shows immunofluorescence images of the microtubule network of fixed PTK2 cells using ATTO647N-labeled secondary antibodies. As expected, STED microscopy enables imaging of the microtubule network with improved resolution under both buffer conditions (compare Figure 1b,d and c,e). The difference in photostability of the fluorophores under the two media becomes apparent in series of scans of the same area. After a single scan, the overall normalized fluorescence is only about 63% of the original value using Mowiol, whereas almost no intensity change is observed when applying the ROXS. After three scans, the Mowiol sample is degraded to below 20% of the original brightness, whereas in the ROXS sample the fluorescence brightness remains at  $\approx 70\%$  (compare Figure 1f and g). The dramatic improvement in photostability is especially important for repetitive measurements to achieve dynamic information,<sup>[21]</sup> or for 3D imaging, in which minute increments in axial direction lead to significant overlap of the focal volumes.

Encouraged by the increased photostability, we tested the ability of successive STED imaging of single ATTO647N molecules under ROXS conditions. ATTO647N-labeled 60-bp double-stranded oligonucleotides (corresponding to a tether length of  $\approx 20$  nm) were immobilized under aqueous conditions via biotin/streptavidin binding. Figure 2 shows alternating confocal and STED images of single ATTO647N molecules immobilized in phosphate-buffered saline (PBS) in the absence and presence of a ROXS and enzymatic oxygen removal. First, the sample was imaged in the confocal mode, that is, without STED, followed by a second scan of the same area with the STED beam overlaid. Figure 2a and b clearly demonstrates the resolution increase obtained at the single-molecule level. In the third scan, the STED beam was turned off again to allow assessment of the number of molecules that survived the STED scanning experiment. This procedure is justified since the

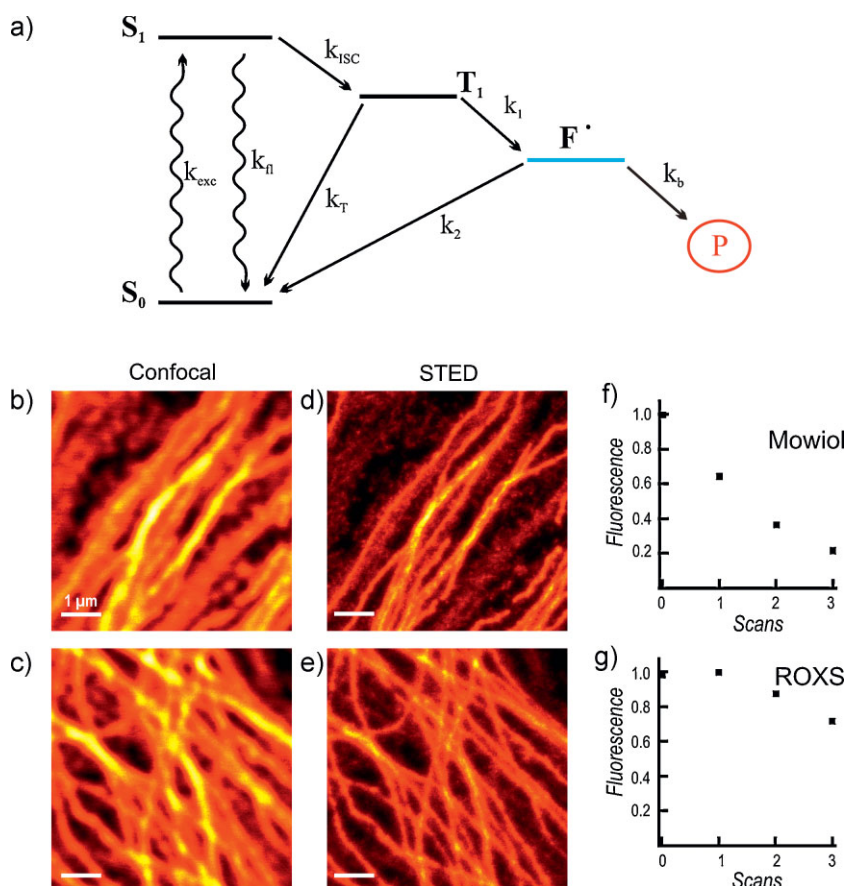


**Figure 1.** a) Jablonski scheme of the ROXS principle. The fluorophore is excited with rate  $k_{exc}$  and fluoresces with rate  $k_f$ ; dependent on the intersystem crossing rate,  $k_{ISC}$ , the triplet state  $T_1$  is populated. The triplet state is efficiently quenched by a reducing or oxidizing compound present in the  $\mu\text{M}$  to  $\text{mM}$  concentration range to produce a radical-ion state with rate  $k_1$  and to repopulate the ground state with rate  $k_2$ . Reverse intersystem crossing ( $k_T$ ) and irreversible photobleaching ( $k_b$ ) compete with the ROXS mechanism. b–e) Immunofluorescence images of the microtubule network of fixed PTK2 cells. The secondary antibody was labeled with a degree of labeling of 4–6 ATTO647N fluorophores per antibody ( $P_{exc} = 2.8 \mu\text{W}$ ,  $P_{STED} = 165 \text{ mW}$ ,  $\lambda_{STED} = 760 \text{ nm}$ ). Measurement sequences were taken on cells embedded in Mowiol (b,d) and ROXS (c,e). The raw data are shown for the confocal and STED modes (scale bars:  $1 \mu\text{m}$ ). f,g) Normalized overall fluorescence intensities of the original scans (shown in b–e) and for three successive scans. In the presence of the ROXS buffer, the fluorescence brightness decreases only 30% after three scans in contrast to an 80% decrease of the original brightness in the case of Mowiol.

number of molecules bleached during the low-excitation-intensity confocal scan is negligible. To visualize the effect of the different buffers, the image of the first scan is color encoded (red) and overlaid with the image of the last scan (blue). Interestingly, some spots appeared only in the second confocal scan (blue spots in Figure 2a) under PBS conditions. Most probably these fluorophores resided in a stable nonfluorescent dark state during the first scan. If the photoinduced process responsible for the formation of such dark states is highly efficient, the fluorophores cannot be detected. The red spots in the right-hand panels of Figure 2a and b visualize STED-induced photobleaching of fluorophores. On the other hand, the purple spots show fluorophores that survived the second scan with the STED beam active. Again, application of the ROXS remarkably increases the photostability of fluorophores under STED conditions, as can be easily recognized by the

larger number of purple spots in the right-hand image in Figure 2b. Additionally, the formation of dark states during image acquisition is strongly reduced by the ROXS.

To unravel the effect of the ROXS, measurements were performed for different STED power levels (Figure 2c). The higher the power of the STED beam, the more cycles a fluorophore has to undergo during image acquisition. Also, it becomes more likely for the fluorophore to cycle in the excited-state system. Thus, a higher resolution is accompanied by an increased probability of photobleaching. At low to moderate STED intensities, the ROXS almost eliminates photobleaching. The number of enduring molecules slowly decreases with increasing STED intensity. Only for the highest STED intensity of 100 mW does photobleaching become significant, with  $\approx 52\%$  of the molecules being photobleached in the presence of the ROXS. At these STED intensities, without the ROXS more than 90% of the molecules are photobleached. The reason for the onset of photobleaching at high STED-beam intensities might be related to the involvement of different bleaching mechanisms, such as singlet-state excitation. While for lower STED intensities photobleaching most probably starts from transient dark states that are efficiently depopulated by the ROXS, at higher STED-beam intensities it becomes more probable that photobleaching occurs directly from the singlet state and higher excited states that evolve out of the singlet state. The ROXS most likely does not prevent these alternative photobleaching pathways.

The fact that a significant fraction ( $\approx 48\%$ ) of fluorophores survives STED-beam average power levels of  $\geq 100 \text{ mW}$

focused onto a doughnut-shaped area of  $\approx 10^{-9} \text{ cm}^2$  enables a study of resolution scaling in STED microscopy using a “true” point source of light under aqueous buffer conditions.<sup>[23]</sup> Figure 3a and b show a STED image and its confocal counterpart, respectively. The dramatic resolution enhancement can easily be seen in the presented raw data. Representative images were taken with a STED power of 63 mW at 750 nm. Typically we achieved a resolution of  $46 \pm 5 \text{ nm}$  with  $597 \pm 17$  photons detected from single immobilized ATTO647N molecules. These parameters allow us to estimate the average (centroid) position of single molecules in the STED image with an accuracy of 1.8 nm (Figure 3c) for single ATTO647N molecules. The measurements shown in Figure 3a and b were used to confirm the resolution scaling of STED microscopy with single fluorophores. For each STED-beam power, at least 20 molecules were picked and their images

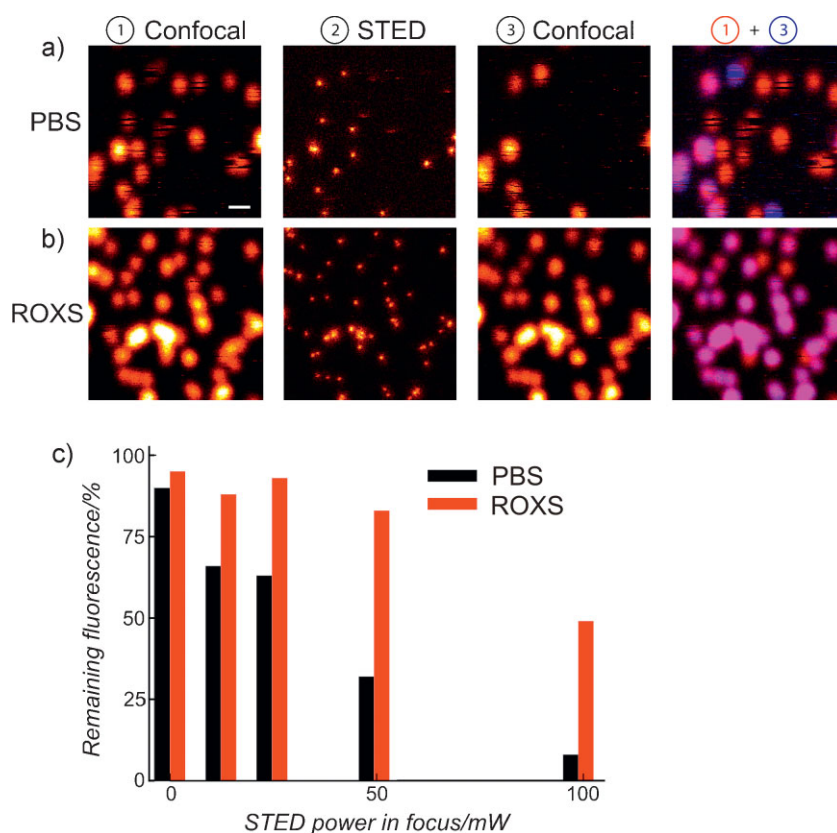


**Figure 2.** a,b) Fluorescence images of single ATTO647N-labeled 60-bp oligonucleotides immobilized under different aqueous buffer conditions in the absence (confocal) and presence of the STED beam (750 nm) with an average power of 49 mW at the sample. To visualize the effect of STED-beam-induced photobleaching, the image of the first scan is color encoded red and overlaid with the image of the third scan in the images shown on the right-hand side in the two panels. Measurements were performed in PBS in the absence (a) and presence (b) of the ROXS (enzymatic oxygen removal and addition of 1 mM methyl viologen and 1 mM Trolox). All data shown are raw. c) Quantitative analysis of the fraction of fluorophores surviving STED microscopy at different powers of the STED beam in the absence and presence of the ROXS.

(i.e., point spread functions (PSFs) of the imaging process) were determined using a two-dimensional Gaussian fit. The mean of the fitted width is plotted against the saturation factor  $\zeta = I_m/I_s$ . The maximum intensity at the doughnut crest,  $I_m$ , is determined from the average power of the STED beam  $P_{STED}$  and the doughnut focal area on the sample. The resolution of the microscope has been measured within the range  $\zeta = 0-125$  corresponding to  $P_{STED} = 0-150$  mW in the focal plane.

In the confocal image, a lateral resolution of 226 nm was determined that improved with increasing  $P_{STED}$  (Figure 3d). Up to  $\zeta \approx 50$ , the resolution nicely obeys the initially discussed inverse square-root law which, for convenient comparison with the confocal microscopy resolution, is used here in a rewritten form:<sup>[2,23]</sup>

$$d = d_c / \sqrt{1 + a^2 \zeta^2} \quad (1)$$

where  $d_c$  is the confocal resolution (in terms of the full width at half maximum, FWHM). The parameter  $a$  characterizes the intensity gradient of the doughnut minimum.<sup>[23]</sup> A fit to the

data yields the parameters  $d_c = 226$  nm and  $a = 0.003$  nm<sup>-1</sup>, which are in good agreement with previous results.<sup>[20]</sup>

Interestingly, the measured resolution values slightly deviate from those expected for the highest saturation factors. A possible explanation represents movement of the fluorophore ATTO647N attached to the bovine serum albumin (BSA)/biotin-covered surface via streptavidin/biotin and a 60-bp-long double-stranded DNA molecule. At this length scale, the DNA strand can to a good approximation be regarded as a rigid 20-nm rod. Consequently, the fluorophore can diffuse on a hemisphere with a radius of approximately 20 nm (see Figure 3e). Therefore, we estimated the influence of the DNA tether on the resolution of STED microscopy, assuming free diffusion on the hemisphere on a timescale significantly faster than data acquisition, that is, all positions on the hemisphere were equally sampled. We then convoluted the expected shape of the effective STED focus with the distribution of molecules on the hemisphere projected onto the surface and determined the resulting FWHM. To fit our data to the observed FWHM values, we used the maximum deviation from the perpendicular DNA orientation (denoted maximum angle in Figure 3e) as fit parameter. For an expected FWHM of 30.3 nm ( $\zeta = 100$ ), an experimental FWHM of  $(38 \pm 2)$  nm was found. In the case of a completely freely moving DNA tether, a FWHM of 44.7 nm was expected. The experimental deviation could be well fitted for a positional distribu-

tion of molecules if a maximum angle of  $53^\circ$  was used as a parameter (see Figure 3d), that is, the model assumes equal distribution of DNA orientations down to an angle of  $37^\circ$  with respect to the surface. Interestingly, the same maximum angle was determined for  $\zeta = 125$ , for which a FWHM of 25.5 nm was expected and  $(35 \pm 4)$  nm was measured. If the broadening of the FWHM is indeed due to the movement of the fluorophore, the necessity to include a minimum angle in our model might indicate that not all positions are equally sampled during the measurement time, either due to specific interactions or to an excluded volume close to the surface, as assumed in the calculation. The estimations indicate, however, that with realistic assumptions the broadening of the FWHM could be related to the DNA length. We therefore used a sample without DNA, that is, the fluorophore was linked to the BSA/streptavidin surface directly as ATTO647N-biotin. Corresponding measurements yielded a better resolution, as indicated by the red data points in Figure 3d, thus reproducing the expected resolution scaling. At  $\zeta = 125$ , a resolution of  $(26 \pm 1)$  nm was experimentally achieved in two dimensions. These data strongly support the idea that the FWHM measured

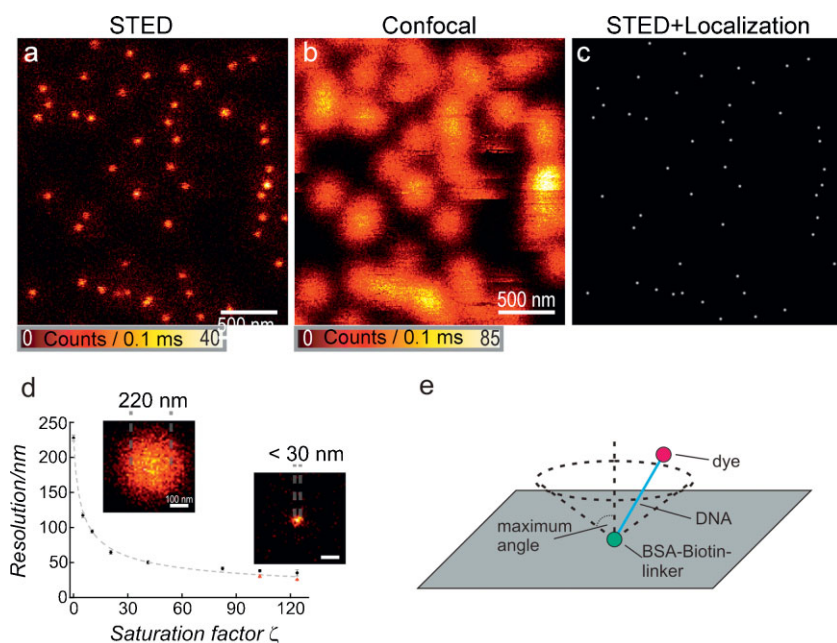


**Figure 3.** a,b) Representative fluorescence images of single immobilized double-stranded 60-bp oligonucleotides labeled with ATTO647N. a) High-resolution STED image. The power of the excitation and STED beams (750 nm) was 5  $\mu$ W and 63 mW in the focal plane, respectively. Raw data are shown. b) Corresponding confocal counterpart. Note that differences in the fluorescence signal in (a) could be due to binding of two DNA strands on the streptavidin linker and in (b) due to summing the PSFs of more than one single molecule not distinguishable in confocal microscopy. c) Marked positions of single fluorophores evaluated from the STED data shown in (a). The center of mass of each single emitter could be localized with less than 2 nm accuracy, since the total number of photons per molecule and scan was around 600 (597  $\pm$  17 photons). For better visualization the positions were marked by a disk 8 nm in diameter. d) Resolution at different saturation factors as controlled by the STED-beam power. The two red data points in the curve are from measurements with directly immobilized fluorophores using ATTO647N–biotin instead of 60-bp double-stranded oligonucleotides. The fit of Equation (1) to the data is shown as a dashed gray line, which demonstrates that the oligonucleotide linker length of 20.4 nm limits the resolution to  $\approx$ 35 nm for single ATTO647N molecules. Hence the measured highest resolution is not limited by the limited power of STED but by molecular movement. e) Scheme of the model used to estimate the influence of the linker length on resolution. Comparing (a)–(c), note the dramatic improvement in molecular-transition-based far-field optical resolution.

in our experiments is influenced by the movement of the fluorophore and depends on the way the fluorophore is immobilized on the surface.

In summary, we synergistically combined two important advances in fluorescence microscopy, namely resolution and signal increase, by applying a ROXS to STED microscopy. Adding a ROXS shortens the lifetime of the triplet state, identified as the major bleaching pathway in STED microscopy.<sup>[13]</sup> We have shown that this combination leads to a several-fold improvement of the signal, practically achievable resolution, and sample lifetime, which are important for many in vitro nanoscopy applications. Resolution scaling has been demonstrated using single molecules as point sources in two dimensions under biologically relevant conditions down to a resolution of <30 nm. Deviations of the expected resolution scaling for high STED-beam intensities could be attributed to the length and flexibility of the DNA tether used. Measurements without a DNA tether confirm that under the applied optical conditions, the resolution increases down to

values of <30 nm. Importantly, the method introduced is not restricted to the use of ATTO647N. Carbo-cyanines, such as Cy5 and Alexa 647, and other standard fluorophores also show a dramatic increase in photostability and fluorescence intensity upon application of a ROXS.<sup>[14]</sup> Since less toxic ROXS systems, such as a combination of Trolox and Trolox-quinone<sup>[15]</sup> or glutathione and oxygen, are available,<sup>[16,18]</sup> the application of a ROXS in live-cell microscopy may also become possible in the near future.

## Experimental Section

**Materials:** ATTO647N was purchased from ATTO-TEC (Siegen, Germany) as *N*-hydroxysuccinimidyl ester (NHS-ester) for covalent coupling to amino-modified oligonucleotides (from IBA, Göttingen, Germany). The sequence of the 60-bp double-stranded DNA employed is published elsewhere.<sup>[24,25]</sup>

**Synthesis of fluorophore-labeled oligonucleotides:** Labeling of the amino-modified oligonucleotides with the fluorescent dye was performed by classical NHS-ester chemistry using standard solvents purchased from Merck (Darmstadt, Germany). A fivefold excess of NHS-ester was added to one mole equivalent of oligonucleotide dissolved in 0.1 M carbonate buffer (pH 9.4), and the mixture was incubated for 6 h while protected from light. Labeled oligonucleotides were purified by HPLC (Hewlett Packard, Böblingen, Germany) using a reversed-phase column (Knauer, Berlin, Germany) of octadecylsilane-Hypersil C18. Separation was performed in 0.1 M triethylammonium acetate with a linear gradient from 0 to 75% acetonitrile over 20 min.

**Immobilization of labeled DNA:** Cover slides were incubated with HF ( $\approx$ 1%) for 20 s and rinsed with water. The slides were incubated overnight with a BSA/BSA-biotin solution (BSA 7.5 mg mL<sup>-1</sup>; BSA-biotin 1 mg mL<sup>-1</sup>). After three washing steps with PBS and addition of streptavidin (0.2 mg mL<sup>-1</sup>) over 5 min, the system was ready for immobilization of biotinylated DNA strands. Double-stranded DNA containing a biotin tag at the 3' end of the template strand was immobilized on streptavidin-coated surfaces as described elsewhere.<sup>[22]</sup> Measurements were performed in PBS unless stated otherwise. In cases in which oxygen was removed from the solution, an enzymatic oxygen-scavenging system was applied that contained 10% (w/v) glucose, 12.5% (v/v) glycerol, glucose oxidase (30  $\mu$ g mL<sup>-1</sup>), catalase (3  $\mu$ g mL<sup>-1</sup>), and 0.4–0.8 mM tris(2-carboxyethyl)phosphine hydrochloride (TCEP). For measurements with ATTO647N directly linked to biotin, the same immobilization technique as described above was used, but instead of incubating the prepared surface with biotinylated double-stranded DNA labeled with ATTO647N, the ATTO647N–biotin construct was used.

**Sample preparation cells:** The mammalian PtK2 cell line was grown as described previously.<sup>[26]</sup> Cells were seeded on standard glass coverslips to a confluence of about 80% and fixed with ice-cold methanol (−20 °C) for 4 min followed by incubation in blocking buffer (PBS containing 1% BSA). Immunostaining of microtubules was performed with anti- $\beta$ -tubulin mouse immunoglobulin G (IgG; Sigma) as primary antibody and with ATTO647N-conjugated sheep antimouse IgG as secondary antibody. Both antibodies were diluted in blocking buffer and incubated for 1 h each followed by several washes in blocking buffer.

**Single-molecule fluorescence experiments:** The STED setup used for the high-resolution measurements has been described before.<sup>[23,27]</sup> Pulsed excitation was implemented by a 635 nm laser diode (Picoquant GmbH, Germany). It was triggered by the photodiode signal of the STED laser (MIRA 900, Coherent, USA) operating at 750 nm. The doughnut-shaped intensity distribution used for the STED beam was achieved by adding a phase plate with helical phase retardation (RPC Photonics, Rochester, NY, USA) to the STED beam. Detection of the fluorescent photons was performed by an avalanche photodetector (APD, Perkin Elmer) coupled to a multimode fiber acting as the confocal pinhole (0.7 times Airy disks).

### Keywords:

fluorescence · imaging · photostability · redox chemistry · stimulated emission depletion microscopy

- [1] S. W. Hell, J. Wichmann, *Opt. Lett.* **1994**, *19*, 780–782.
- [2] V. Westphal, S. W. Hell, *Phys. Rev. Lett.* **2005**, *94*, 143903.
- [3] M. Heilemann, S. van de Linde, M. Schuttpelz, R. Kasper, B. Seefeldt, A. Mukherjee, P. Tinnefeld, M. Sauer, *Angew. Chem.* **2008**, *120*, 6266–6271; *Angew. Chem. Int. Ed.* **2008**, *47*, 6172–6176.
- [4] B. Huang, W. Wang, M. Bates, X. Zhuang, *Science* **2008**, *319*, 810–813.
- [5] L. Schermelleh, P. M. Carlton, S. Haase, L. Shao, L. Winoto, P. Kner, B. Burke, M. C. Cardoso, D. A. Agard, M. G. Gustafsson, H. Leonhardt, J. W. Sedat, *Science* **2008**, *320*, 1332–1336.
- [6] H. Shroff, C. G. Galbraith, J. A. Galbraith, E. Betzig, *Nat. Methods* **2008**, *5*, 417–423.
- [7] G. Shtengel, J. A. Galbraith, C. G. Galbraith, J. Lippincott-Schwartz, J. M. Gillette, S. Manley, R. Sougrat, C. M. Waterman, P. Kanchanawong, M. W. Davidson, R. D. Fetter, H. F. Hess, *Proc. Natl. Acad. Sci. USA* **2009**, *106*, 3125–3130.
- [8] S. W. Hell, *Science* **2007**, *316*, 1153–1158.
- [9] M. Heilemann, P. Dedecker, J. Hofkens, M. Sauer, *Laser Photonics Rev.* **2009**, *3*, 180–202.
- [10] P. Tinnefeld, M. Sauer, *Angew. Chem.* **2005**, *117*, 2698–2728; *Angew. Chem. Int. Ed.* **2005**, *44*, 2642–2671.
- [11] J. P. Hoogenboom, E. M. H. P. van Dijk, J. Hernando, N. F. van Hulst, M. Garcia-Parajo, *Phys. Rev. Lett.* **2005**, *95*, 097401.
- [12] J. Widengren, A. Chmyrov, C. Eggeling, P.-A. Löfdahl, C. A. M. Seidel, *J. Phys. Chem. A* **2007**, *111*, 429–440.
- [13] G. Donnert, J. Keller, R. Medda, M. A. Andrei, S. O. Rizzoli, R. Lurmann, R. Jahn, C. Eggeling, S. W. Hell, *Proc. Natl. Acad. Sci. USA* **2006**, *103*, 11440–11445.
- [14] J. Vogelsang, R. Kasper, C. Steinhauer, B. Person, M. Heilemann, M. Sauer, P. Tinnefeld, *Angew. Chem.* **2008**, *120*, 5545–5550; *Angew. Chem. Int. Ed.* **2008**, *47*, 5465–5469.
- [15] T. Cordes, J. Vogelsang, P. Tinnefeld, *J. Am. Chem. Soc.* **2009**, *131*, 5018–5019.
- [16] S. van de Linde, R. Kasper, M. Heilemann, M. Sauer, *Appl. Phys. B* **2008**, *93*, 725–731.
- [17] C. Steinhauer, C. Forthmann, J. Vogelsang, P. Tinnefeld, *J. Am. Chem. Soc.* **2008**, *130*, 16840–16841.
- [18] M. Heilemann, S. van de Linde, A. Mukherjee, M. Sauer, *Angew. Chem.* **2009**, *48*, 7036–7041; *Angew. Chem. Int. Ed.* **2009**, *48*, 6903–6908.
- [19] S. van de Linde, U. Endesfelder, A. Mukherjee, M. Schuttpelz, G. Wiebusch, S. Wolter, M. Heilemann, M. Sauer, *Photochem. Photobiol. Sci.* **2009**, *8*, 465–469.
- [20] J. Vogelsang, T. Cordes, C. Forthmann, C. Steinhauer, P. Tinnefeld, *Proc. Natl. Acad. Sci. USA* **2009**, *106*, 8107–8112.
- [21] V. Westphal, S. O. Rizzoli, M. A. Lauterbach, D. Kamin, R. Jahn, S. W. Hell, *Science* **2008**, *320*, 246–249.
- [22] K. I. Willig, S. O. Rizzoli, V. Westphal, R. Jahn, S. W. Hell, *Nature* **2006**, *440*, 935–939.
- [23] B. Harke, J. Keller, C. K. Ullal, V. Westphal, A. Schonle, S. W. Hell, *Opt. Express* **2008**, *16*, 4154–4162.
- [24] M. Heilemann, E. Margeat, R. Kasper, M. Sauer, P. Tinnefeld, *J. Am. Chem. Soc.* **2005**, *127*, 3801–3806.
- [25] M. Heilemann, R. Kasper, P. Tinnefeld, M. Sauer, *J. Am. Chem. Soc.* **2006**, *128*, 16864–16875.
- [26] K. Weber, T. Bibring, M. Osborn, *Exp. Cell Res.* **1975**, *95*, 111–120.
- [27] B. Harke, C. K. Ullal, J. Keller, S. W. Hell, *Nano Lett.* **2008**, *8*, 1309–1313.

Received: February 8, 2010  
 Revised: April 2, 2010  
 Published online: June 2, 2010